ELSEVIER

Polymer 43 (2002) 5915–5933

polymer

www.elsevier.com/locate/polymer

Effect of organoclay structure on nylon 6 nanocomposite morphology and properties

T.D. Fornes[a*], P.J. Yoon[a], D.L. Hunter[b], H. Keskkula[a], D.R. Paul[a,*]

[a]*Department of Chemical Engineering, Texas Materials Institute, University of Texas at Austin, Austin, TX 78712-1062, USA*
[b]*Southern Clay Products, 1212 Church Street, Gonzales, TX 78629, USA*

Received 17 April 2002; received in revised form 12 June 2002; accepted 14 June 2002

Abstract

A carefully selected series of organic amine salts were ion exchanged with sodium montmorillonite to form organoclays varying in amine structure or exchange level relative to the clay. Each organoclay was melt-mixed with a high molecular grade of nylon 6 (HMW) using a twin screw extruder; some organoclays were also mixed with a low molecular grade of nylon 6 (LMW). Wide angle X-ray scattering, transmission electron microscopy, and stress–strain behavior were used to evaluate the effect of amine structure on nanocomposite morphology and physical properties. Three surfactant structural issues were found to significantly affect nanocomposite morphology and properties in the case of the HMW nylon 6: decreasing the number of long alkyl tails from two to one tallows, use of methyl rather than hydroxy-ethyl groups, and use of an equivalent amount of surfactant with the montmorillonite, as opposed to adding excess, lead to greater extents of silicate platelet exfoliation, increased moduli, higher yield strengths, and lower elongation at break. LMW nanocomposites exhibited similar surfactant structure-nanocomposite behavior. Overall, nanocomposites based on HMW nylon 6 exhibited higher extents of platelet exfoliation and better mechanical properties than nanocomposites formed from the LMW polyamide, regardless of the organoclay used. This trend is attributed to the higher melt viscosity and consequently the higher shear stresses generated during melt processing. © 2002 Published by Elsevier Science Ltd.

Keywords: Nylon 6; Nanocomposites; Melt processing

1. Introduction

Interest in polymer layered silicate nanocomposites is driven by the possibility of exceptional physical property enhancements, e.g. increased modulus and improved barrier properties, at low filler levels. The key to such performance rests in the ability to exfoliate and disperse individual, high-aspect ratio silicate platelets within the polymer matrix. Recent studies have explored achieving exfoliated structures from organoclays in a wide range of polymer matrices using a variety of processing routes [1]. To date, well-exfoliated composites have been achieved in only a selected number of polymers, viz., nylon 6 [2–5], polystyrene [6], certain polyimides [7–9] and epoxies [10–12]. Of these, nylon 6 is particularly unique since exfoliated nanocomposites have been formed by more than one processing technique, i.e. in situ polymerization [2,3] and melt processing in a well-designed twin screw extruder [4,5,13]. The technique of melt processing is particularly attractive due to its versatility and compatibility with existing processing infrastructure and is beginning to be used for commercial applications [14–16].

Recent work in this laboratory has focused on the effects of processing conditions, polymer structure and rheology, and the structure of the organic modifier of the clay on the formation of polymer nanocomposites via melt processing. For nylon 6, the extruder must be optimized with regard to both shear intensity and residence time to achieve high levels of clay platelet exfoliation [17]. Use of high molecular weight nylon 6 leads to much better exfoliation owing to the high shear stresses in the extruder that result from its high melt viscosity [18,19]. Limited results suggest that the nature of the organic component, or 'surfactant', on the organoclay may also be a key factor.

Reichert et al. investigated how the length of the alkyl group on the amine used to modify sodium fluoromica and addition of maleated polypropylene (PP-*g*-MA) affected the

* Corresponding authors. Tel.: +1-512-471-5392; fax: +1-512-471-0542.
E-mail addresses: drp@che.utexas.edu (D.R. Paul), timothy@che.utexas.edu (T.D. Fornes).

0032-3861/02/$ - see front matter © 2002 Published by Elsevier Science Ltd.
PII: S0032-3861(02)00400-7

morphology and mechanical properties of polypropylene nanocomposites formed by melt processing [20]. A critical alkyl length of 12 carbons or more was found necessary for promoting exfoliation in conjunction with PP-*g*-MA. Increasing the anhydride functionality of PP-*g*-MA also promoted exfoliation.

There is also evidence that surfactant structure affects the extent of exfoliation achieved by the in situ polymerization technique. For example, Usuki et al. showed that swelling of montmorillonite modified with ω-amino acids by ε-caprolactam increased significantly when the carbon number of the amino acid was greater than 8 [21,22]. This ultimately led to the selection of the proper amino acid needed to form the exfoliated nanocomposite described in the literature as NCH [2,3], which is now a commercial product of Ube Industries Ltd (Japan). In addition, Usuki et al. compared four types of inorganic silicates: montmorillonite, synthetic mica, saponite, and hectorite. They discovered that clays having higher exchange capacities, i.e. montmorillonite and synthetic mica, lead to more efficient exfoliation of the silicate platelets.

Lan et al. described how the structure of the organic modifier of the clay, as well as the clay itself, influenced exfoliation in epoxy nanocomposites [23]. They found that use of alkyl ammonium cations with chain lengths longer than eight carbons, high acidity of the onium ion, and clays with low to intermediate charge density led to greater extents of exfoliation. The latter observation is counter to other results [22] and may be due to differences in the nature of the bond between polymer segments and the organic surfactant, i.e. secondary bonding as opposed to covalent bonding, respectively. At this point, the available literature does not allow one to generalize the relationship between organoclay structure, nanocomposite morphology, and the processing route.

The objective of this paper is to examine the relationship between the structure of the organic cation on the organoclay and the morphology and properties of nylon 6 nanocomposites formed by melt processing. Specific comparisons among organic amine surfactants that are potentially available from commercial sources will be made by addressing structural variations one issue at a time. Wide angle X-ray scattering (WAXS), transmission electron microscopy (TEM), and stress–strain behavior are used to evaluate nanocomposite morphology and physical properties. A subsequent paper will focus on color formation and polymer matrix molecular weight degradation issues associated with the organic component.

2. Experimental

2.1. Nylon 6 materials

Two commercial grades of nylon 6 from Honeywell (formerly AlliedSignal), a high molecular weight grade (Capron® B135WP, with $M_n = 29\,300$) and low molecular weight grade (Capron® 8202 with $M_n = 16\,400$), were used in this study. Further details of these materials are reported elsewhere [18,19]. The high and low molecular weight polyamides will be referred to as HMW and LMW, respectively.

2.2. Melt processing

Melt blended nanocomposites were formed using a Haake co-rotating twin screw extruder with the barrel temperature set at 240 °C, a screw speed of 280 rpm, and a feed rate of 980 g/h as described previously [18,19]. Prior to extrusion, organoclay powder and nylon 6 were thoroughly mixed in a 3 L container and placed into the hopper of a screw feeder. The amount of montmorillonite (MMT) in each extruder batch was determined by placing pre-dried nanocomposite pellets in a furnace at 900 °C for 45 min and weighing the remaining MMT ash. A correction for loss of structural water is made in the calculation [18,19].

Extruded nanocomposites pellets were dried and then injection molded into standard tensile bars (ASTM D638, Type I) in an Arburg Allrounder 305-210-700 injection molding machine using a barrel temperature of 260 °C, mold temperature of 80 °C, injection pressure of 70 bar, and a holding pressure of 35 bar.

2.3. Mechanical testing

Tensile tests were performed according to ASTM D638 using an Instron model 1137 upgraded for computerized data acquisition. Modulus and yield strength were determined using an extensometer at a crosshead speed of 0.51 cm/min. Elongation at break was measured at a speeds of 0.51 and 5.1 cm/min from total crosshead travel using a value of 9.04 cm for the gage length. Tensile property values reported here represent an average for six specimens; standard deviations were typically of the order of 4% for modulus, 1% for yield strength, and between 5 and 25% for elongation at break.

2.4. Wide angle X-ray scattering

WAXS scans, conducted in reflection mode at a scan rate of 1°/min, were performed on a Sintag XDS 2000 diffractometer using Ni filtered Cu Kα X-ray radiation ($\lambda = 1.54$ Å) for organoclay powder and injection molded nanocomposites samples taken from the end tab of a tensile bar. Tensile bar specimens were oriented such that the incident beam reflected off the transverse face.

2.5. Transmission electron microscopy

Samples for TEM analysis were taken from compression molded films formed at 240 °C from approximately 10 g of dried nanocomposite pellets using a Wabash compression

press. Ultra thin sections, approximately 70–90 nm thick cut from the molded film, were placed on 300 mesh grids and examined by TEM using a Phillips/EM 301 microscope operating at an acceleration voltage of 80 kV.

2.6. Differential scanning calorimetry

Thermograms were performed on organoclay powder using a Perkin–Elmer DSC 7. Samples were held at 0 °C for 2 min and then heated to 125 °C at a rate of 10 °C/min.

3. Organic modifier structure and characterization

Fig. 1(a) shows the various amine compounds that were exchanged for the sodium ion of native montmorillonite clay (CEC = 92 mequiv./100 g clay). A simple nomenclature system for the organic cation is used in Fig. 1(a) to describe its chemical structure in a concise manner. The letters M, H, and (HE) represent methyl, hydrogen, and 2-hydroxy-ethyl substituents, while C*, T, R, and HT, represent units derived from natural products that consist of a distribution of saturated and unsaturated long chain hydrocarbon units: C* denotes the product made from coconut oil which consists predominantly of chains with 12 carbons (~48%); T is for tallow which is predominantly composed of chains with 18 carbons (~65%); R is for rapeseed which consists largely of chains with 22 carbons (~45%). The term HT denotes the tallow-based product in which the majority of the double bonds have been hydrogenated. Further details about the level of unsaturation of these materials are given in a subsequent paper [24]. For convenience, these hydrocarbon chains are often referred to here as 'alkyls' whether saturated or not.

These amine compounds, originally supplied by Akzo Nobel to Southern Clay Products, are ion exchanged with sodium montmorillonite by one of two schemes, depending upon their structure. Quaternary-based clays, i.e. the top six structures in Fig. 1(a), are formed by first dispersing sodium montmorillonite in water at 80 °C, followed by the addition of the quaternary ammonium chloride. Tertiary amines, such as $M_2H_1(HT)_1$ and $M_1H_1(HT)_2$, require protonation before the ion exchange reaction can occur. This is achieved by adding sulfuric acid to the reaction medium containing dispersed montmorillonite, water, and the tertiary amine. The reaction product is filtered, dried, and milled, eventually resulting in organoclay powder. It should be noted that in either reaction the amine compound is typically added in stoichiometric proportion to that of the cation exchange capacity (CEC) of the clay. In some cases, excess amounts of amine are added to over-saturate the montmorillonite galleries. The level of amine added to the clay is designated by the milliequivalent ratio (MER).

The amine compounds were carefully chosen to explore the relationship between the chemical structure of the cation and the morphology and properties of nanocomposites

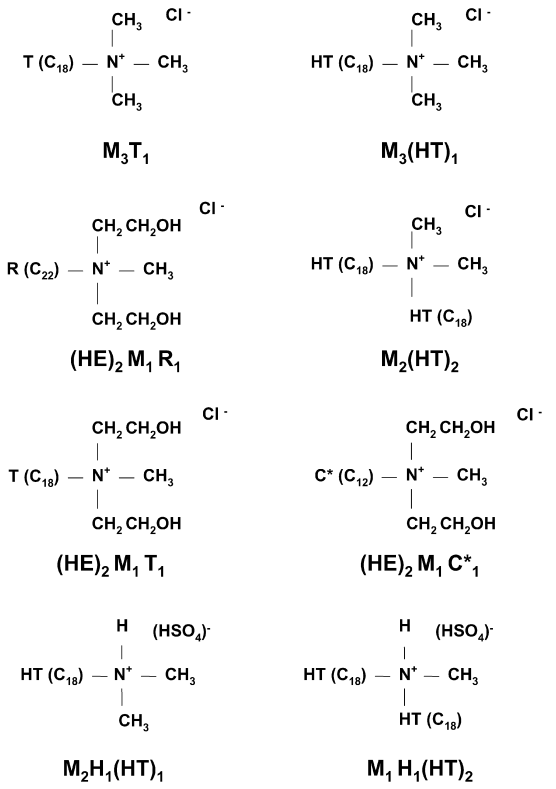

(a)

Effect	Organoclays		
Number of Alkyl Tails	$M_3(HT)_1$	*vs.*	$M_2(HT)_2$-95
	$M_2H_1(HT)_1$	*vs.*	$M_1H_1(HT)_2$
Hydroxy-ethyl vs. Methyl	M_3T_1	*vs.*	$(HE)_2M_1T_1$
MER Loading	$M_2(HT)_2$-95	*vs.*	$M_2(HT)_2$-125
Quaternary vs. Tertiary	$M_3(HT)_1$	*vs.*	$M_2H_1(HT)_1$
	$M_2(HT)_2$-95	*vs.*	$M_1H_1(HT)_2$
Saturation	M_3T_1	*vs.*	$M_3(HT)_1$
Length of Alkyl Tail	$(HE)_2M_1C^*_1$		
	$(HE)_2M_1T_1$		
	$(HE)_2M_1R_1$		

(b)

Fig. 1. (a) Molecular structure and nomenclature of amine salts used to organically modify sodium montmorillonite by ion exchange. The symbols M: methyl, T: tallow, HT: hydrogenated tallow, HE: 2-hydroxy-ethyl, R: rapeseed, C*: coco, and H: hydrogen designate the substituents on the nitrogen. (b) Organoclays used to evaluate the effect of structural variations of the amine cations on nanocomposite morphology and properties.

Table 1
Organoclays used in this study

Organoclay[a]	SCP designation[b]	Chemical structure	Specifications[c]
$(HE)_2M_1R_1$	Experimental	bis(2-hydroxy-ethyl)methyl rapeseed ammonium montmorillonite	95 MER, Organic content = 34.1 wt%, d_{001} spacing = 18.0 Å
$(HE)_2M_1C_1^*$	Experimental	bis(2-hydroxy-ethyl)methyl coco ammonium montmorillonite	95 MER, Organic content = 26.4 wt%, d_{001} spacing = 15.2 Å
$(HE)_2M_1T_1$	Cloisite® 30B	bis(2-hydroxy-ethyl)methyl tallow ammonium montmorillonite	90 MER, Organic content = 31.5 wt%, d_{001} spacing = 17.9 Å
M_3T_1	Experimental	Trimethyl tallow quaternary ammonium montmorillonite	95 MER, Organic content = 29.1 wt%, d_{001} spacing = 17.8 Å
$M_3(HT)_1$	Experimental	Trimethyl hydrogenated-tallow ammonium montmorillonite	95 MER, Organic content = 29.6 wt%, d_{001} spacing = 18.0 Å
$M_2H_1(HT)_1$	Experimental	Dimethyl hydrogenated-tallow ammonium montmorillonite	95 MER, Organic content = 28.9 wt%, d_{001} spacing = 17.1 Å
$M_1H_1(HT)_2$	Experimental	Methyl bis(hydrogenated-tallow) ammonium montmorillonite	95 MER, Organic content = 38.4 wt%, d_{001} spacing = 24.3 Å
$M_2(HT)_2$-95	Cloisite® 20A	Dimethyl bis(hydrogenated-tallow) ammonium montmorillonite	95 MER, Organic content = 39.6 wt%, d_{001} spacing = 24.2 Å
$M_2(HT)_2$-125	Cloisite® 15A	Dimethyl bis(hydrogenated-tallow) ammonium montmorillonite	125 MER, Organic content = 45.1 wt%, d_{001} spacing = 32.3 Å

[a] The substituents on the tertiary and quaternary ammonium compounds used to form the above organoclays are identified in the following shorthand notation: C*: coco, R: rapeseed, T: tallow, HT: hydrogenated-tallow, HE: 2-hydroxy-ethyl, M: methyl, H: hydrogen. Coco, rapeseed, and tallow are natural products composed predominantly of unsaturated C_{12} alkyl chains (48%), C_{22} alkyl chains (45%), and C_{18} alkyl chains (65%), respectively.
[b] Commercial designations provided by Southern Clay Products, Inc.
[c] The organic loading is a quantity describing the number of milliequivalents of amine salt used per 100 g of clay (MER) during the cationic exchange reaction with sodium montmorillonite. The wt% of organic component on the final organoclay was determined by high temperature residual ash measurements. The basal spacing corresponds to the characteristic Bragg reflection peak (d_{001}) obtained from a powder WAXS scan of the organoclay.

formed from the corresponding organoclays. The selection of amines shown in Fig. 1(a) permits six structural comparisons to be made one variable at a time as presented in Fig. 1(b). Details of the nine organoclays used here are listed in Table 1. The organoclay designations $M_2(HT)_2$-95 and $M_2(HT)_2$-125 represent two different MER loading levels; the first is a stoichiometric loading, while the latter is an over-exchanged clay having excess amine within the clay galleries. The amines used to form these organoclays are representative of commercially available intermediates that can be produced in large quantities at relatively low costs. On the other hand, the amines used in many studies have more well-defined structures with nearly pure *n*-alkyl units, but organoclays formed from these may be prohibitively expensive.

Fig. 2(a) illustrates WAXS scans for three organoclays, $M_1H_1(HT)_2$, $(HE)_2M_1T_1$, and $M_2H_1(HT)_1$, and pristine sodium montmorillonite, NaMMT.[1] These results show that replacing the sodium ions with large ammonium cations results in increased *d*-spacings. In addition, larger substituents on the ammonium ion leads to higher *d*-spacings (lower 2θ angles) for the organoclay. In other words, the montmorillonite gallery expands as needed to accommodate more intercalated material. For the organoclays in which the MER level is the same, this is a direct consequence of the number average molecular weight of the gallery cation,[2] as shown in Fig. 2(b). This physical effect may be better visualized by plotting basal spacing versus the mass of organic component per unit mass of inorganic MMT for each organoclay, as shown in Fig. 2(c). These data can be analyzed in more detail to gain insight about how the intercalated alkyl ammonium ions pack in the gallery. The mass of organic material per unit volume of gallery, or gallery density, can be expressed as

$$\rho_{\text{gallery}} = \frac{\text{mass organic}}{\text{gallery volume}} = \frac{1}{(d-d_0)} \frac{(\text{mass organic}/\text{mass MMT})}{\left(\frac{\text{area}/\text{side}}{\text{mass MMT}}\right)} \quad (1)$$

where $d - d_0$ is the gallery height as indicated by the schematic in Fig. 2(c). The second term in the denominator is calculated from the specific surface area to be 750 m^2/g for sodium montmorillonite [25]. The numerator is determined by residual ash measurements obtained after high temperature burn off of the organoclay, as outlined in Section 2. The slope of the linear relation between gallery height and the second quantity in Eq. (1) gives the density of the organic material in the gallery, ρ_{gallery}. A simple, unconstrained least squares fit of a straight line through

[1] Sodium montmorillonite powder was dried at 110 °C for 24 h prior to the X-ray analysis in order to remove any intercalated water.
[2] The number average molecular weight of the ammonium ions was calculated using compositional analysis data of the natural products, coconut oil, tallow, and rapeseed, obtained from Akzo Nobel Chemicals.

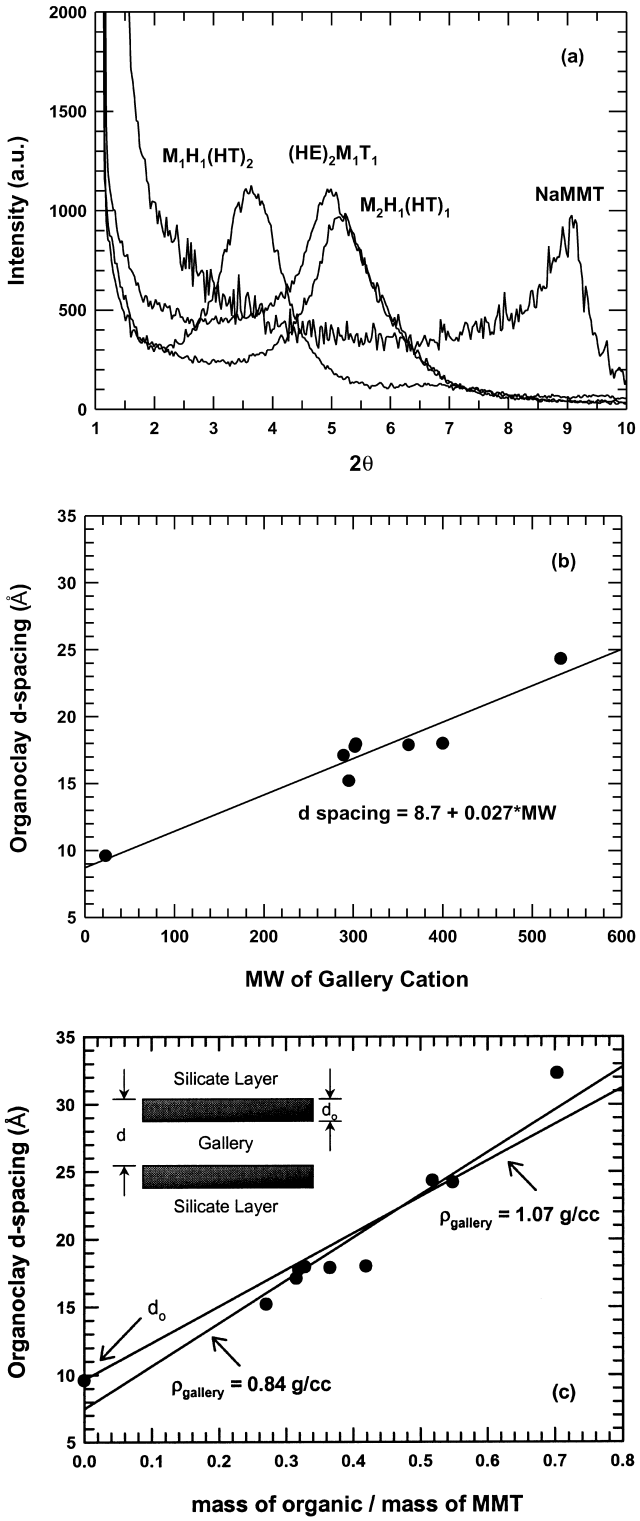

Fig. 2. WAXS results for organoclays. (a) Sample plots of intensity versus 2θ for $M_1H_1(HT)_2$, $(HE)_2M_1T_1$, and $M_2H_1(HT)_1$ organoclays and sodium montmorillonite, NaMMT, and *d*-spacing of all organoclays as a function of (b) number average molecular weight of the gallery cation and (c) mass of organic per unit mass of montmorillonite. The NaMMT curve has been magnified to the approximately the same intensity level as the organoclay curves.

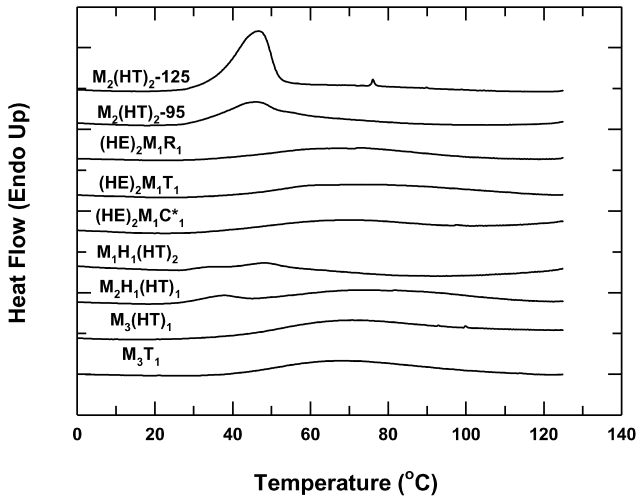

Fig. 3. Differential scanning calorimetry results for organoclay powder.

these data lead to a density of 0.84 g/cm^3. This fit gives an intercept of $d_0 = 7.5$ Å; whereas, the basal spacing of pristine sodium montmorillonite is 9.6 Å. The thickness of a montmorillonite platelet should be slightly less than the observed basal spacing of 9.6 Å since the associated sodium ions occupy some volume and force the MMT platelets apart by some amount; however, this effect is not enough to justify an intercept of 7.5 Å. Alternatively, forcing the fit through an intercept of $d_0 = 9.6$ Å produces a calculated density of 1.07 g/cm^3. This range of densities encompasses what might be expected for organic liquids or solids. The densities calculated here agree with conclusions made by Vaia et al. about the conformation and structure of the organic interlayer of similar organoclays [26]. Using infrared spectroscopy and X-ray diffraction techniques, they found that organoclay galleries exhibit molecular environments ranging from solid- to liquid-like.

Differential scanning calorimetry of these organoclays do indeed reveal both non-crystalline and crystalline behavior as seen in Fig. 3. Organoclays such as $M_2(HT)_2$-95 and $M_2(HT)_2$-125 display broad endothermic peaks around 47 °C, while the remaining organoclays are absent of any significant peaks. The lack of a significant endothermic transition may be due to the presence of double bonds in the long hydrocarbon chains and the size distribution of the chains. In the case of the over-exchanged, $M_2(HT)_2$-125 organoclay, a secondary minor peak exists around 76 °C, which is near the melting temperature of free surfactant as reported by Gelfer et al. [27]. The extremely broad peaks visible in many of these clays may reflect desorption of small amounts of water on the clay.

4. Mechanical property analysis

Comparison of properties of nanocomposites formed from the different organoclays should be made at a fixed montmorillonite content, rather than at a fixed organoclay

content, since the silicate portion of the organoclay is the reinforcing component. Therefore, mechanical property data are plotted versus weight percent MMT. Fig. 4 shows the relationship between modulus and montmorillonite content for all the nanocomposites prepared in this study based on the high molecular weight nylon 6 material mentioned earlier (solid points). The vertical spread in these data indicate the extent that organoclay structure affects the level of reinforcement. The solid lines in Fig. 4 were drawn to bracket the upper and lower extremes of stiffness enhancement. For comparison, a single data point is shown for the commercial nanocomposite formed by in situ polymerization [5,28], designated as Ube NCH2. Pellets of the latter were injection molded into tensile bars and tested using the same experimental protocol as described earlier. Its modulus (triangle) lies in the middle of the range for nanocomposites formed by melt processing. This demonstrates that melt processing can lead to comparable, if not better, stiffness properties than composites formed by in situ polymerization.

To see the effects of the structure of the amine compound on the nanocomposite morphology and properties, it is important that comparisons be made at precisely fixed MMT contents. The current experimental design included two target MMT loading levels, 2.9 and 4.5 wt% MMT (see dashed lines in Fig. 4). However, due to limitations in the feeding equipment system used for extrusion at the time of these experiments, these targets could not be precisely maintained from one nanocomposite batch to the next, as seen in Fig. 4.[3] Therefore, in order to best evaluate structure–property effects, it is necessary to interpolate/extrapolate mechanical property data to the target loadings of 2.9 and 4.5 wt% MMT. Modulus versus MMT content is assumed to be linear over the range 2.8 and 4.9 wt% MMT. Yield strength data are non-linear with respect to wt% MMT and were best represented by a second-order polynomial over the range of MMT concentrations (i.e. from 0 to ~5 wt% MMT). Elongation data were well fitted by a declining exponential function. In some cases, elongation data at MMT concentrations of ~1.5 and 7 wt% MMT previously reported were used to better interpolate/extrapolate the current data [18,19]. Overall, curve fitting was quite satisfactory with average coefficients of determination of $R^2 = 0.98$, 0.99, and 0.91 for modulus, yield strength, and elongation at break, respectively. Tables 2 and 3 summarize the raw and interpolated/extrapolated mechanical property data for nanocomposites based on HMW nylon 6.

Finally, before conclusions could be drawn about structure–property relations, it is necessary to assess the extent of statistical uncertainty between replicate batches. Table 4 lists the reproducibility of measured MMT content and mechanical properties results for four extrusions using HMW nylon 6 and $(HE)_2M_1C_1^*$. Each MMT value represents an average of four measurements, while modulus, yield strength, and elongation at break represent an average of seven measurements. The grand average and standard deviation are the statistical results for lumping all individual MMT and mechanical measurements into a combined data set. The grand standard deviation is used to determine whether or not two property values are significantly different using a student's t test at a 90% confidence interval [29].

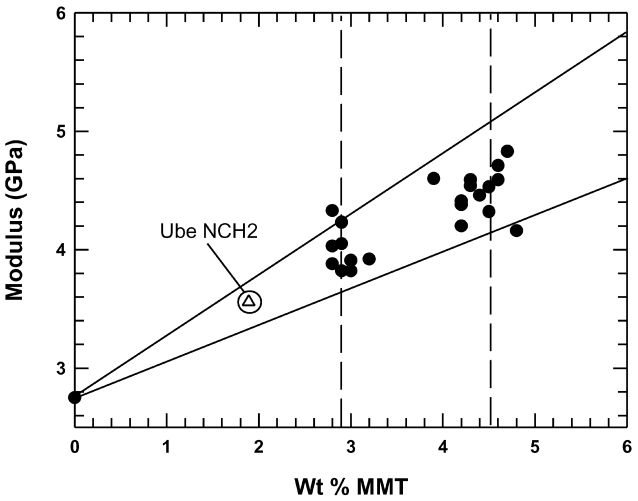

Fig. 4. Modulus as a function of montmorillonite content of nanocomposites formed from HMW nylon 6 (black circles) made by melt processing using a twin screw extruder. The triangle represents the NCH2 nanocomposite from Ube Industries formed by in situ polymerization. NCH2 pellets were injection molded and subsequently tested using the same experimental protocol as what used for the melt processed nanocomposites. The dashed vertical lines represent experimental target MMT loading levels in wt%.

5. Effects of organoclay structure on nanocomposite morphology and mechanical properties

5.1. Organoclay physical structure

There are suggestions in the literature that the extent of exfoliation of an organoclay in a polymer matrix should relate to the basal spacing of the organoclay. For example, Reichert et al. indirectly showed a gradual increase in tensile modulus with organoclay d-spacing, caused by the increase in the carbon number of the alkyl substituent on the onium ion, for a PP/PP-MA/modified MMT system [20]. They found a gradual increase in tensile modulus as alkyl chain length was increased from a carbon number of four to eight carbons. Increasing the alkyl length from 8 to 12 carbons resulted in a significant increase in d-spacing and a step increase in modulus. However, modulus leveled off

[3] The use of one feeder to simultaneously feed polymer pellet–organoclay powder mixtures made it difficult to control the level of MMT from one extrusion batch to the next. To address this problem, an additional feeder strictly for feeding organoclay has been added to the extrusion process. Future melt processing work will be executed with this new feeder setup.

Table 2
Experimental mechanical property data for nanocomposites formed from HMW nylon 6 and various organoclays

HMW–organoclay nanocomposite	Modulus (GPa)	Yield strength (MPa)	Elongation at break (%)	
			Crosshead speed, 0.51 cm/min	Crosshead speed, 5.1 cm/min
Virgin HMW nylon 6–0.0 wt% MMT	2.75	69.7	304	129
$(HE)_2M_1R_1$–3.2 wt% MMT	3.92	84.9	120	27
$(HE)_2M_1R_1$–4.6 wt% MMT	4.59	91.3	39	25
$(HE)_2M_1C_1^*$–2.9 wt% MMT[a]	3.82	85.8	188	45
$(HE)_2M_1C_1^*$–4.2 wt% MMT	4.41	92.0	32	13
$(HE)_2M_1T_1$–2.8 wt% MMT	4.03	85.9	172	36
$(HE)_2M_1T_1$–4.2 wt% MMT	4.38	90.1	97	15
M_3T_1–2.8 wt% MMT	4.33	86.3	87	16
M_3T_1–3.9 wt% MMT	4.60	92.1	15	9.1
M_3T_1–4.7 wt% MMT	4.83	90.0	19	14
$M_3(HT)_1$–2.9 wt% MMT	4.23	85.2	153	31
$M_3(HT)_1$–4.3 wt% MMT	4.54	90.9	–	23
$M_3(HT)_1$–4.6 wt% MMT	4.71	90.7	10	16
$M_2H_1(HT)_1$–2.8 wt% MMT	3.88	87.5	81	22
$M_2H_1(HT)_1$–2.9 wt% MMT	4.05	84.5	173	32
$M_2H_1(HT)_1$–4.3 wt% MMT	4.59	91.6	17	8.9
$M_2H_1(HT)_1$–4.5 wt% MMT	4.53	89.3	40	21
$M_1H_1(HT)_2$–3.0 wt% MMT	3.91	84.8	181	30
$M_1H_1(HT)_2$–4.2 wt% MMT	4.20	87.6	–	22
$M_1H_1(HT)_2$–4.4 wt% MMT	4.46	84.9	13	7.5
$M_2(HT)_2$-95–3.0 wt% MMT	3.82	84.5	174	42
$M_2(HT)_2$-95–4.5 wt% MMT	4.32	87.7	60	28
$M_2(HT)_2$-125–3.0 wt% MMT	3.82	80.3	–	29
$M_2(HT)_2$-125–4.8 wt% MMT	4.16	82.0	142	29

[a] This data set represents an average of four runs (Table 4).

beyond a carbon number of 12. Similar conclusions have been made by Lan and Pinnavaia for epoxy-based nanocomposites [11]. In general, one might expect that larger initial layer spacings may lead to easier exfoliation since platelet–platelet attraction is reduced. It is implied that diffusion of polymer chains inside clay galleries is less hindered due to increased spacing and ultimately leads to improved exfoliation. This represents an oversimplified picture since exfoliation is highly dependent upon a variety of factors, e.g. thermodynamic interactions (polymer–clay,

Table 3
Mechanical property data for nanocomposites formed from HMW nylon 6 and various organoclays interpolated or extrapolated to the targeted MMT loading levels

HMW–organoclay nanocomposite	Modulus (GPa)	Yield strength (MPa)	Elongation at break (%)	
			Crosshead speed (0.51 cm/min)	Crosshead speed (5.1 cm/min)
$(HE)_2M_1R_1$–2.9 wt% MMT	3.77	83.5	120	46
$(HE)_2M_1R_1$–4.5 wt% MMT	4.54	90.8	51	27
$(HE)_2M_1C_1^*$–2.9 wt% MMT	3.90	86.7	125	46
$(HE)_2M_1C_1^*$–4.5 wt% MMT	4.54	93.1	55	27
$(HE)_2M_1T_1$–2.9 wt% MMT	4.06	86.4	147	46
$(HE)_2M_1T_1$–4.5 wt% MMT	4.46	90.8	97	27
M_3T_1–2.9 wt% MMT	4.36	87.9	50	22
M_3T_1–4.5 wt% MMT	4.77	90.9	18	9.4
$M_3(HT)_1$–2.9 wt% MMT	4.22	85.4	98	36
$M_3(HT)_1$–4.5 wt% MMT	4.65	90.9	18	18
$M_2H_1(HT)_1$–2.9 wt% MMT	4.00	89.0	52	21
$M_2H_1(HT)_1$–4.5 wt% MMT	4.60	90.9	18	7.6
$M_1H_1(HT)_2$–2.9 wt% MMT	3.86	84.9	106	28
$M_1H_1(HT)_2$–4.5 wt% MMT	4.42	85.9	52	12
$M_2(HT)_2$-95–2.9 wt% MMT	3.79	84.2	128	46
$M_2(HT)_2$-95–4.5 wt% MMT	4.32	87.7	75	27
$M_2(HT)_2$-125–2.9 wt% MMT	3.80	80.2	188	43
$M_2(HT)_2$-125–4.5 wt% MMT	4.10	82.0	115	25

Table 4
Reproducibility of MMT loading and mechanical properties of nanocomposites formed from HMW nylon 6 and $(HE)_2M_1C^*$

Run no.	MMT level (wt%)		Modulus (GPa)		Yield strength (MPa)		Elongation at break (5.1 cm/min) (%)	
	Average	SD	Average	SD	Average	SD	Average	SD
1	2.81	0.03	3.85	0.14	85.4	0.5	45.7	15.4
2	2.64	0.03	3.81	0.18	85.6	1.0	48.8	8.3
3	2.79	0.04	3.86	0.16	86.1	0.5	47.3	9.9
4	2.60	0.01	3.77	0.11	86.3	0.7	40.0	5.9
Grand statistics	2.71	0.10	3.82	0.15	85.8	0.8	45.4	10.8

polymer–surfactant, and clay–clay), organoclay stability, packing density, etc.

To examine the effect of organoclay physical structure on mechanical properties, current modulus and yield strength data were plotted versus organoclay basal spacing. Fig. 5 reveals a slight downward trend in stiffness and strength with increasing layer spacing at both MMT concentrations.

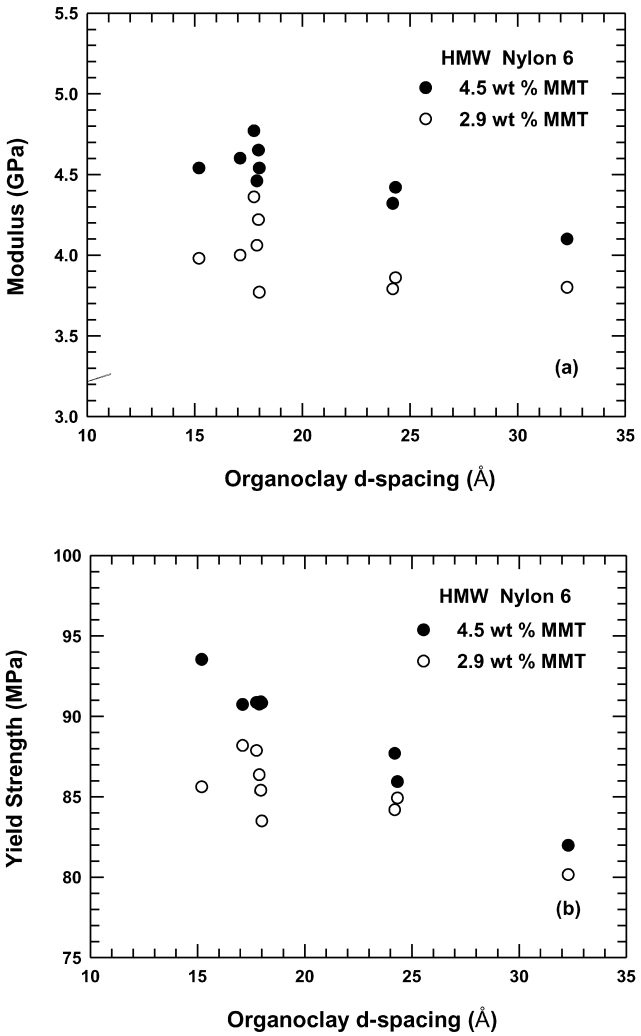

Fig. 5. Effect of organoclay *d*-spacing on nanocomposite (a) modulus and (b) yield strength at the targeted MMT concentrations of 2.9 and 4.5 wt%; all data for HMW nylon 6.

The even larger negative slope in the yield strength plot, Fig. 5(b), could suggest a decrease in interfacial strength, in addition to less exfoliation. Overall, these responses differ from previously reported results as mentioned earlier; in the final analysis such trends may be more reflective of changes in surface chemistry of the organoclay than simply platelet separation. Since the two are interrelated, it is difficult to decouple them.

5.2. Organoclay chemical structure

In what follows, we will attempt to isolate, one variable at a time, the effect of organic modifier structure on the mechanical properties of the resulting nanocomposites using WAXS and TEM as characterization tools for assessing the extent of platelet exfoliation. Mechanical property plots in this section are based on data from Table 3. Of the various mechanical properties determined, modulus is the best indicator of clay platelet exfoliation and will be heavily weighted for gauging effects of modifier structure on exfoliation. Yield strength generally follows modulus effects, increasing with increasing stiffness, as shown in Fig. 6. However, yield strength may also reflect changes in interfacial strength between the matrix and the clay. It is well-known in conventional composites that interfacial

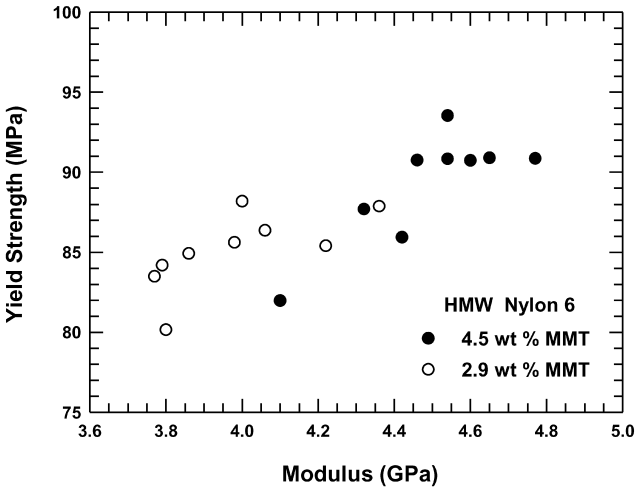

Fig. 6. Relationship between yield strength and modulus for nanocomposites containing MMT concentrations of 2.9 and 4.5 wt%.

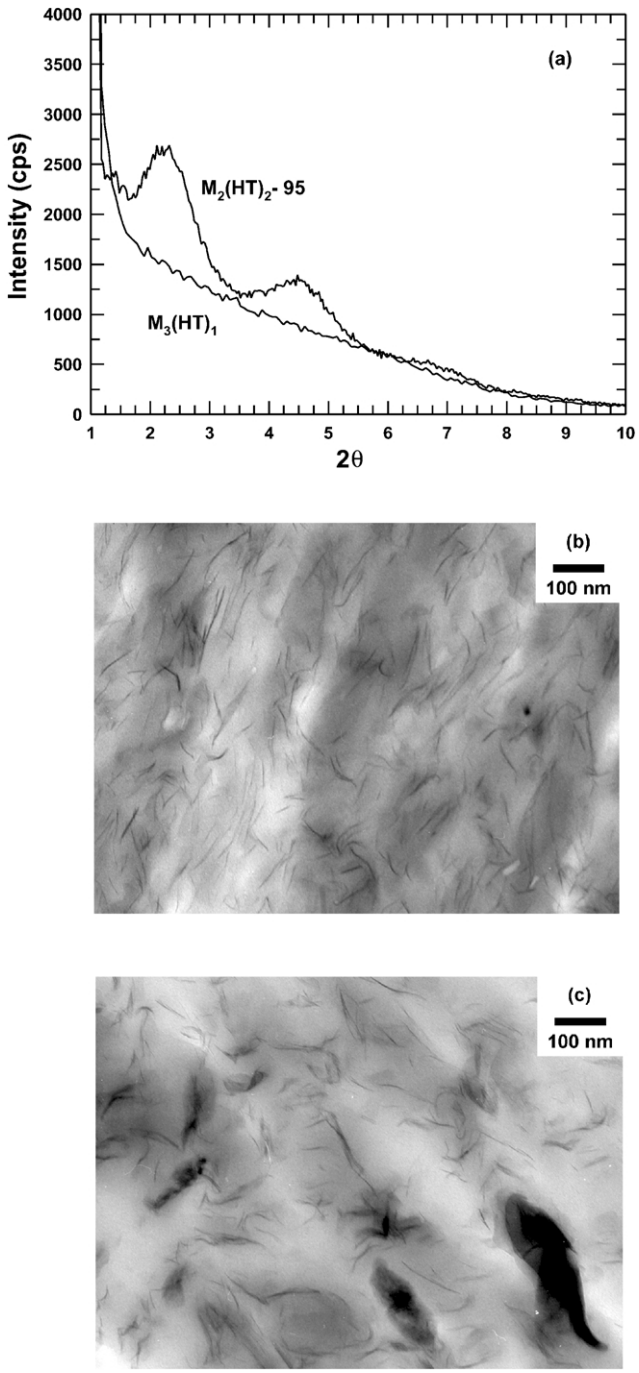

Fig. 7. Morphological analysis of nanocomposites based on HMW nylon 6 and the organoclays $M_3(HT)_1$ and $M_2(HT)_2$-95. (a) WAXS scans and TEM photomicrographs of (b) $M_3(HT)_1$ and (c) $M_2(HT)_2$-95 based composites. The concentrations of MMT in the $M_3(HT)_1$ and $M_2(HT)_2$-95 nanocomposites are 2.9 and 3.0 wt%, respectively.

adhesion has a strong effect on strength; on the other hand, modulus is much less affected by the nature of the interface [30,31].

5.2.1. Effect of number of long alkyl groups

Fig. 7 shows WAXS and TEM results for comparing the morphology of nanocomposites formed from HMW nylon 6 and the organoclays $M_3(HT)_1$ and $M_2(HT)_2$-95, thus, showing the effect of having one versus two long alkyl groups on the quaternary amine. The nanocomposite derived from the one-tailed hydrogenated tallow organoclay has no characteristic X-ray reflections (Fig. 7(a)), which suggests a highly exfoliated structure containing dispersed silicate platelets. The nanocomposite based on the two-tailed amine, on the other hand, has a peak at approximately $2\theta = 2.15°$, which corresponds to an interlayer spacing of 41 Å. This spacing is approximately 17 Å larger than the basal spacing of the pristine organoclay, indicating the presence of a population of polymer intercalated tactoids. The TEM photomicrographs in Fig. 7(b) and (c) corroborate the WAXS results. The nanocomposite from $M_3(HT)_1$ consists predominantly of exfoliated MMT platelets (Fig. 7(b)), while the composite from the $M_2(HT)_2$-95 organoclay contains a large number of multi-layered stacks of clay platelets intercalated with polymer and a smaller number of dispersed features, with one or two silicate layers (Fig. 7(c)).

The mechanical properties of the two types of nanocomposites parallel the X-ray and TEM results. Fig. 8(a) shows that the organoclay from $M_3(HT)_1$ leads to a much higher level of reinforcement than that from the two-tailed $M_2(HT)_2$-95 clay. Student's *t*-tests indicate that the differences in modulus are quite significant at both MMT loadings. Elongation at break data, presented in Fig. 8(a′), show that the more exfoliated $M_3(HT)_1$ system is less ductile than the $M_2(HT)_2$-95 system; generally, ductility decreases when stiffness is increased by reinforcement.

Another 'one tail' versus 'two tails' comparison can be made using the tertiary amine versions of the above organoclays. Fig. 9(a) shows WAXS scans for nanocomposites based on $M_2H_1(HT)_1$ and $M_1H_1(HT)_2$; both seem to have an exfoliated structure since there are no diffraction peaks. Indeed, the respective TEM photomicrographs in Fig. 9(b) and (c) reveal well-exfoliated structures containing dispersed layer(s) of MMT. However, the TEM image for the two-tailed $M_1H_1(HT)_2$ composite, Fig. 9(c), appears to have a smaller number of platelets per unit area on average than the one-tailed TEM image, Fig. 9(b). This difference is also apparent in the mechanical properties of the two nanocomposites. Fig. 8(b) shows that the one-tailed $M_2H_1(HT)_1$ nanocomposite exhibits higher moduli than the two-tailed $M_1H_1(HT)_2$ nanocomposites by a statistically significant margin. The one-tailed material has lower elongation at break values than the two-tailed system, as seen in Fig. 8(b′).

Based on the above results, it is concluded that organoclays made from amines containing one long alkyl group lead to better exfoliation of the montmorillonite platelets and subsequently greater stiffness than surfactants containing two long alkyl groups when all other aspects of the structure are the same. These observations are believed to stem from differences in access of polyamide segments to the silicate surface permitted by the two structures. Nylon 6

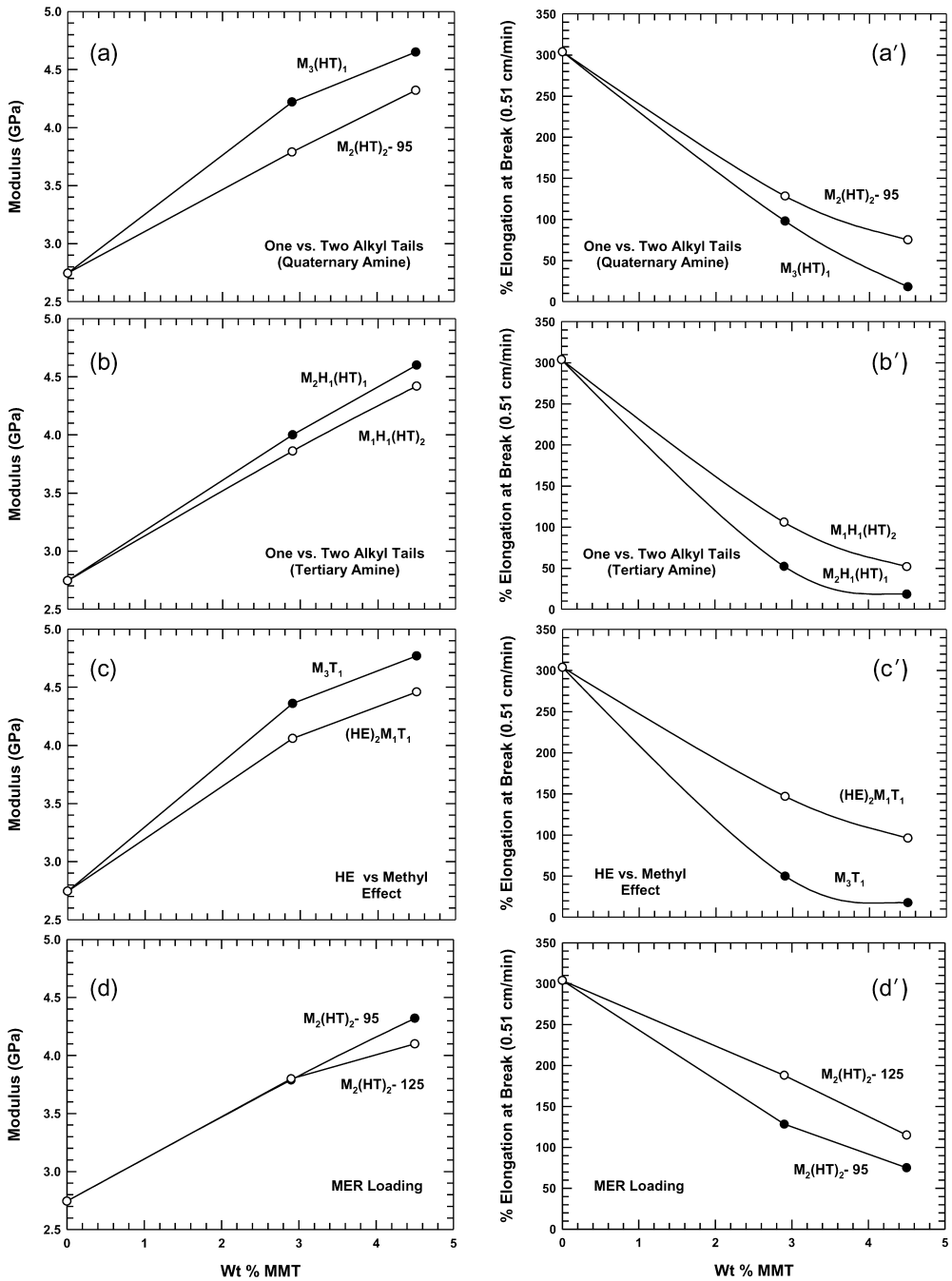

Fig. 8. Modulus (left) and elongation at break (right) of nanocomposites based on HMW nylon 6 and organoclays showing the effects of (a,a′) quaternary amines having one versus two alkyl tails, (b,b′) tertiary amines having one versus two alkyl tails, (c,c′) the effect of 2-hydroxy-ethyl versus methyl groups, and (d,d′) the effect of MER loading.

is a relatively polar polymer also capable of high degrees of hydrogen bonding. We propose that the polyamide has a relatively good affinity for the polar surface of the MMT. A surfactant with two long aliphatic tails limits the access of the nylon 6 segments to the silicate surface more than a one-tailed system, thereby shielding polyamide–MMT interactions and creating a more hydrocarbon-like environment at the organoclay surface. This agrees with the thermodynamic analysis and molecular modeling of Vaia and Giannelis [32,33] and Tanaka and Goettler [34]. Based on their lattice model of polymer of melt intercalation, Vaia and Giannelis conclude that desirable changes in interactions energies are achievable through the maximization of the number of favorable polymer–silicate interactions and the minimization of unfavorable non-polar interactions between polymer and alkyl type surfactants on the silicate. This favorable interaction is believed to provide the driving force for polymer intercalation and aids subsequent

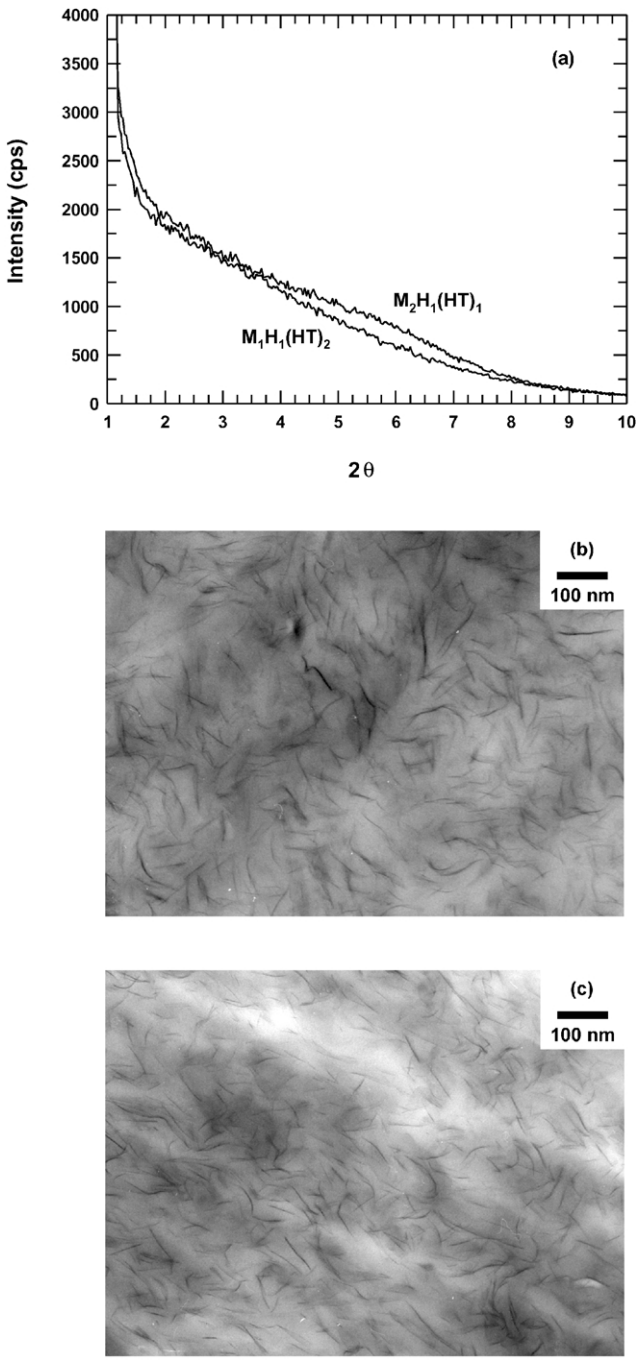

Fig. 9. Morphological analysis of nanocomposites based on HMW nylon 6 and the organoclays $M_2H_1(HT)_1$ and $M_1H_1(HT)_2$. (a) WAXS scans and TEM photomicrographs of (b) $M_2H_1(HT)_1$, and (c) $M_1H_1(HT)_2$ based composites. The concentrations of MMT in the $M_2H_1(HT)_1$ and $M_1H_1(HT)_2$ nanocomposites are 2.8 and 3.0 wt%, respectively.

exfoliation. Tanaka and Goettler predicted binding energies for polyamide nanocomposites by molecular modeling. Their results show that the surfactant shields interactions between the polyamide and the clay and that larger surfactant molecules result in larger shielding effects. The polyamide–clay binding energy was found to decrease from a maximum value for polyamide with pristine clay as the molecular volume of the surfactant increased.

In addition to these studies, Masenelli-Varlot et al. report mechanical property data for melt processed nanocomposites formed from nylon 6 and organoclays having one and two octadecyl groups on the amine that agree with the results reported here [35]. Nanocomposites derived from the two-tailed amine structure resulted in intercalated composites having moderate stiffness improvements relative virgin nylon 6, while the one-tailed structure leads to good exfoliation of montmorillonite and superior nanocomposite moduli. Elongation at breaks were higher for the composites based on the two-tailed amine as compared to composites based on one long alkyl tail, a trend also observed in the present study.

5.2.2. Hydroxy-ethyl versus methyl

Fig. 10(a) shows WAXS scans for nanocomposites based on organoclays with and without 2-hydroxyl-ethyl substituents, i.e. $(HE)_2M_1T_1$ and M_3T_1. Both show a relatively smooth decline of intensity with 2θ implying that the organoclay is delaminated and well dispersed. There is a quite small peak in the M_3T_1 scan occurring around $2\theta = 6°$ corresponding to a basal spacing of 14.7 Å. This spacing is slightly less than that of the repeat spacing of the pristine M_3T_1 organoclay. This may be due to the collapse of a small fraction of the organoclay galleries caused by onium ion degradation. The TEM photomicrographs of the two nanocomposites in Fig. 10(b) and (c) reveal exfoliated morphologies in support of the WAXS results. The features present in both photomicrographs range from individual silicate platelets to small intercalated stacks containing two to three platelets. Overall, there appears to be little difference between the two images.

The mechanical properties, however, do provide a meaningful differentiation between the two structures as seen in Fig. 8(c); having two methyl groups leads to a higher modulus than simply having two hydroxy-ethyl substituents on the ammonium ion. Fig. 8(c′) shows that the $(HE)_2M_1T_1$ based nanocomposite has a higher elongation at break than the M_3T_1 composite, as would be expected. The difference in exfoliation reflected in the mechanical properties may stem from the relative amount of shielding of the desirable polyamide–silicate interaction. The hydroxy-ethyl groups no doubt occupy more surface space than the methyl substituents. In addition, the –OH moiety may prefer to reside flat on the surface due to attraction to oxygen atoms on the clay. Reducing the number of direct polyamide–clay contacts ultimately leads to a reduction in the level of platelet exfoliation.

5.2.3. Level of organic loading (MER comparison)

Fig. 11(a) shows the effect of excess amine surfactant on the WAXS of nanocomposites formed from $M_2(HT)_2$ organoclays. The X-ray scans for both $M_2(HT)_2$-95 and $M_2(HT)_2$-125 exhibit strong basal reflections at approximately 2.15° ($d_{001} = 41$ Å) and 2.4° ($d_{001} = 37$ Å), respectively. Although the two nanocomposites have nearly

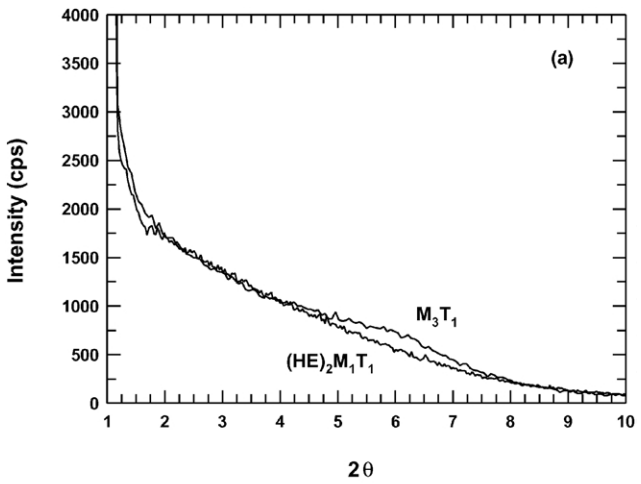

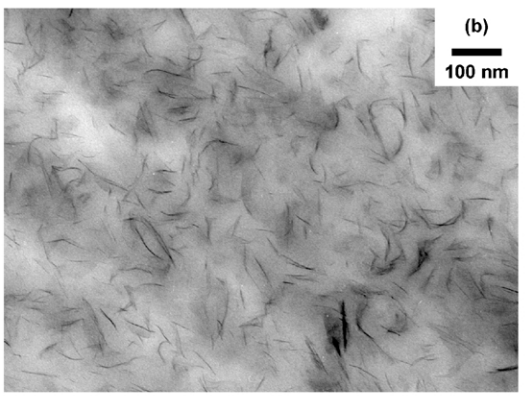

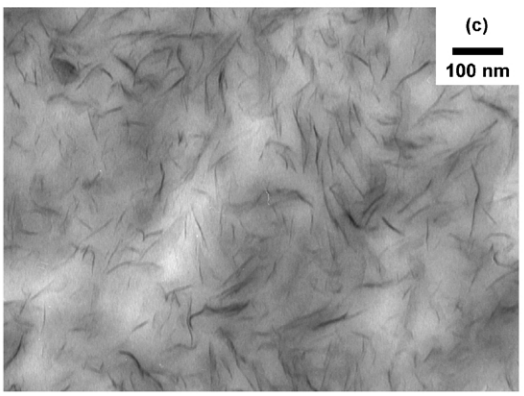

Fig. 10. Morphological analysis of nanocomposites based on HMW nylon 6 and the organoclays $(HE)_2M_1T_1$ and M_3T_1. (a) WAXS scans and TEM photomicrographs of (b) $(HE)_2M_1T_1$, and (c) M_3T_1 based composites. The concentration of MMT in both nanocomposites is 2.8 wt%.

identical scans, it is important to reference these spacings to those of the pristine organoclay spacings of 24.2 and 32.3 Å for $M_2(HT)_2$-95 and $M_2(HT)_2$-125, respectively. This reveals a 17 Å increase in gallery height for the equivalently exchanged organoclay composite, while the over-exchanged system increases only marginally, approximately 4.7 Å. Although the X-ray results indicate that neither organoclay leads to good exfoliation, it seems that excess surfactant is disadvantageous with regard to dispersing

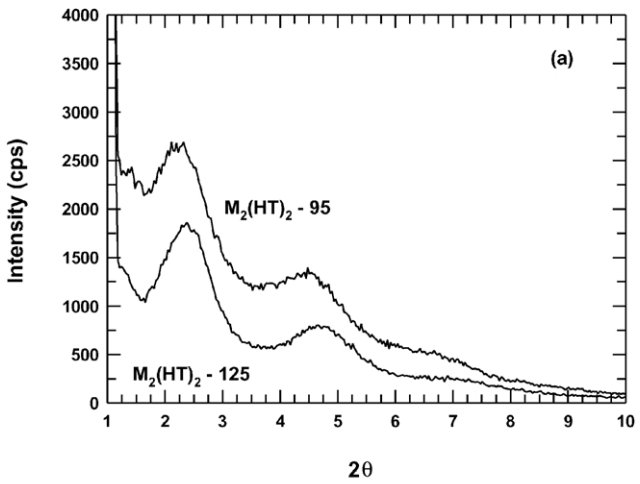

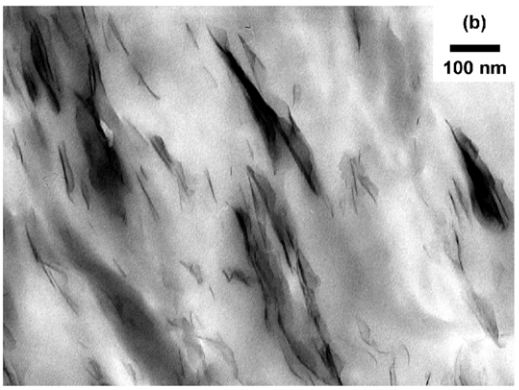

Fig. 11. Morphological analysis of nanocomposites based on HMW nylon 6 and the organoclays $M_2(HT)_2$-95 and $M_2(HT)_2$-125. (a) WAXS scans for $M_2(HT)_2$-95 and $M_2(HT)_2$-125 based composites and TEM photomicrograph of (b) nanocomposite based on $M_2(HT)_2$-125. The concentration of MMT in both nanocomposites is 2.9 wt%. TEM for the nanocomposite based on $M_2(HT)_2$-95 is shown in Fig. 7(c).

MMT platelets. This behavior mirrors the results of Lee et al. for nanocomposites formed from styrene/acrylonitrile copolymers (SAN) and similar $M_2(HT)_2$-based organoclays [36]. They found the 95 MER organoclay was much more efficient in expanding MMT galleries than an over-exchanged one with MER = 140. Their 140 MER organoclay showed little change in basal spacing in the presence of SAN, similar to what was observed here for the 125 MER organoclay and nylon 6. It should be noted that these authors inadvertently confuse the amount of surfactant added during the ion exchange, or MER loading, with the CEC of the montmorillonite; their organoclays were formed from the same montmorillonite used here, whose CEC is fixed.

TEM photomicrographs of the nanocomposites formed from $M_2(HT)_2$-95 and $M_2(HT)_2$-125, respectively, are shown in Figs. 7(c) and 11(b), respectively. The $M_2(HT)_2$-95 composite contains a large fraction of multi-layered stacks of clay platelets intercalated with polymer and a small fraction of dispersed features comprised of one or two layer silicate layers. The $M_2(HT)_2$-125 composite has larger features of either intercalated clay or unaltered stacks of

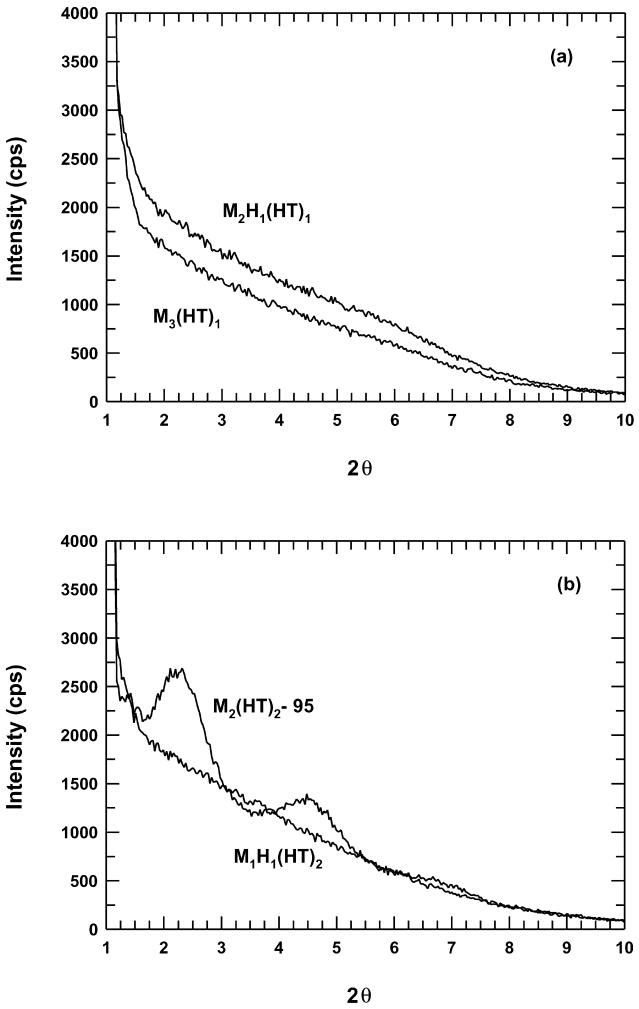

Fig. 12. WAXS scans of nanocomposites based on HMW nylon 6 and quaternary and tertiary organoclays whose ammonium ions having (a) one alkyl and (b) two alkyl tails. The $M_3(HT)_1$, $M_2H_1(HT)_1$, $M_2(HT)_2$-95, and $M_1H_1(HT)_2$ composites contain 2.9, 2.8, 3.0, and 3.0 wt% MMT, respectively.

platelets as well as a minute fraction of dispersed platelets. The nanocomposite made from the higher MER organoclay contains a smaller percentage of individually dispersed platelets and larger interparticle distances, which follows from less platelet exfoliation.

It is interesting to note that the morphology seen by TEM is somewhat different than that predicted by WAXS for the nanocomposite based on the over-exchanged organoclay. Fig. 11(b) indicates the presence of both intercalated structures and delaminated platelets, while the WAXS results above (Fig. 11(a)) would suggest only a low degree of intercalation. It is quite likely that the excess surfactant in the 125 MER organoclay was expelled from the organoclay galleries during extrusion, thus creating a new environment similar to that of the equivalently exchanged clay. If this is the case, then the extent of intercalation of polymer into the clay galleries is underestimated by comparing the *d*-spacing of the nanocomposite to that of the 125 MER organoclay.

Fig. 8(d) shows that MER loading has little effect on modulus at low concentrations of MMT. At higher MMT levels, the organoclay with excess surfactant leads to a slightly lower modulus. The elongation at break is higher for the over-exchanged system at both MMT levels. These effects may reflect plasticization of the matrix by the excess surfactant or simply a lower amount of intercalation or MMT platelet exfoliation. Interestingly, the yield strength of nanocomposites formed from the over-exchanged organoclay is significantly lower than those for composites derived from the equivalently exchanged organoclay (Table 3). This may be caused by a weaker interface between the nylon 6 matrix and the silicate surface, less exfoliation of MMT platelets, and/or by plasticization of the matrix caused by the excess surfactant.

In general, these results would indicate no advantage to using excess surfactant. The inferior morphology and mechanical properties of the over-exchanged system may result from increased coverage of the silicate surface by surfactant thereby reducing the polyamide–clay interaction. However, it may be that the excess $M_2(HT)_2$ surfactant is simply expelled from the clay galleries. If this occurs, then the relative interactions at the organoclay surface should be nearly the same as when there is no excess surfactant. Ultimately, the effect of excess surfactant should be examined using a different amine that tends to give better exfoliation than does $M_2(HT)_2$.

5.2.4. *Quaternary versus tertiary ammonium treatments*

The surfactants in Fig. 1(a) allow two separate comparisons of quaternary versus tertiary amines (Fig. 1(b)). Fig. 12(a) shows that nanocomposites based on quaternary and tertiary organoclays having one hydrogenated tallow tail, i.e. $M_3(HT)_1$ and $M_2H_1(HT)_1$ do not have any WAXS peaks, suggesting that both have exfoliated morphologies. TEM photomicrographs support the conclusions from WAXS as seen in Figs. 7(b) and 9(b). Fig. 12(b) compares WAXS scans of nanocomposites derived from quaternary and tertiary organoclays with amines having two hydrogenated tallow groups. The quaternary-based clay leads to an intercalated morphology, while the tertiary version gives an exfoliated morphology; this is supported by the TEM images seen in Figs. 7(c) and 9(c). It is not fully clear why a methyl versus a hydrogen on the amine leads to such a drastic difference in morphology for these two tail systems. The tertiary amine can be thought of as more polar owing to the acidic hydrogen which might lead to better interaction with the polyamide. However, these effects are not visible in the one-tailed, quaternary versus tertiary organoclay comparison. Perhaps the one-tailed organoclay, due to less surface coverage of silicate, readily exfoliates MMT regardless of whether a methyl or hydrogen substituent is present (e.g. polyamide-clay interactions dominate polyamide–surfactant interactions). Interestingly, studies by Lan et al. have shown that less substituted ammonium ions (e.g. primary and secondary) lead to more exfoliated epoxy-based

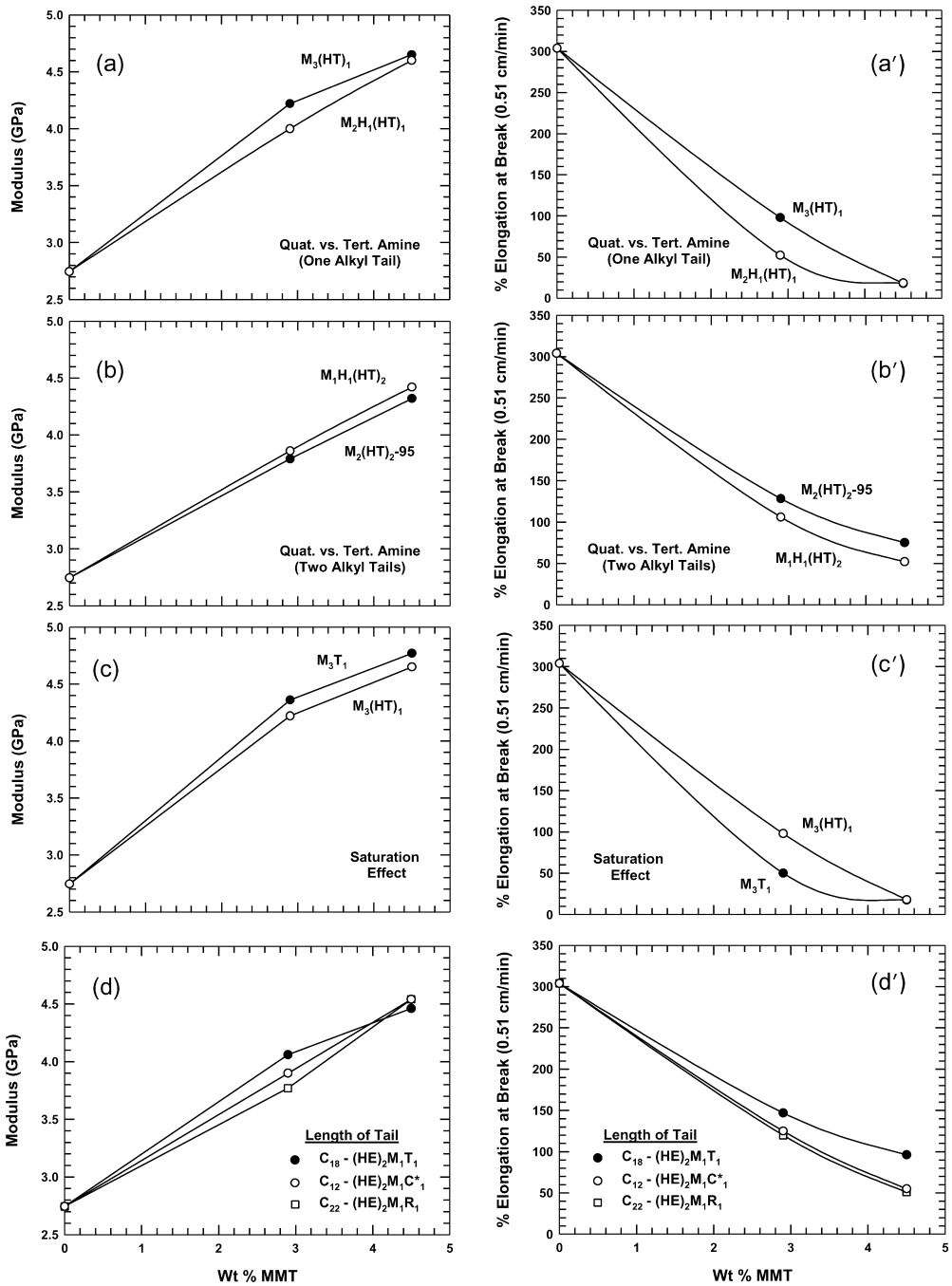

Fig. 13. Modulus (left) and elongation at break (right) of nanocomposites based on HMW nylon 6 and organoclays showing the effects of (a,a′) quaternary versus tertiary amines having one alkyl tail, (b,b′) quaternary versus tertiary amines having two alkyl tails, (c,c′) the effect of unsaturated versus saturated hydrocarbon tails, and (d,d′) the effect alkyl tail length.

nanocomposites than highly substituted ions [23]. They attribute the difference in exfoliation behavior to the level of acidity of the ammonium ion and the catalytic effect this has on the polymerization of the epoxy. Although the results from Lan et al. are similar to the behavior of the above two-tailed quaternary and tertiary HMW systems, it may be unjust to draw any definitive conclusions since these nylon 6 nanocomposites are based on such different chemistry and formation techniques. Evaluation of nanocomposite modulus, Fig. 13(a,a′,b,b′) shows little difference between tertiary and quaternary amines having one or two tallow tails. Statistical *t*-tests reveal at high MMT concentrations modulus values for the one-tailed structures are not significantly which is also the case for modulus values for the two-tailed structures at low concentration MMT. Elongation at break results for both quaternary versus tertiary comparisons show no clear advantage for either type of structure. These data and those given earlier make it

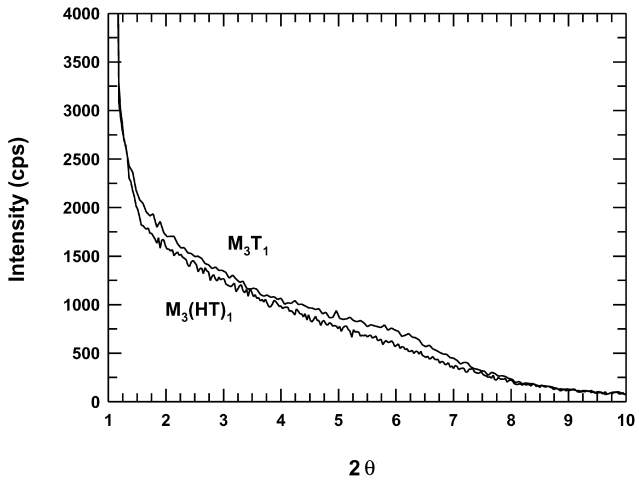

Fig. 14. WAXS scans for HMW nylon 6 nanocomposites formed from the quaternary alkyl ammonium organoclays M_3T_1 and $M_3(HT)_1$, illustrating the effect of hydrogenation of the double bonds on the tallow group. The nanocomposites from the unsaturated and saturated materials contain 2.8 and 2.9 wt% MMT, respectively.

difficult to see any consequences of using quaternary versus tertiary amine surfactants.

5.2.5. Saturated tallow effects

As mentioned in Section 3, the long hydrocarbon tails on the amine surfactants are made from natural products that contain a certain level of unsaturation (i.e. double bonds). In some cases, the double bonds have been hydrogenated. Fig. 14 shows the WAXS spectra for nanocomposites based on the saturated and unsaturated form of tallow, $M_3(HT)_1$ and M_3T_1, respectively. The patterns show no strong Bragg reflections, indicative of exfoliated platelets. The TEM photomicrographs for the two systems indicate exfoliated structures (Figs. 7(b) and 10(c)). Modulus results shown in Fig. 13(c) reveal a slight advantage for the unsaturated clay. Elongation at break results, seen in Fig. 13(c′), are nearly the same for the two composites, particularly at the highest MMT. Based on the above results, hydrogenation of the tallow double bonds seems to have no sizable effect on nanocomposite structure or mechanical properties. However, it has been found that unsaturated organoclays can lead to polymer matrix degradation; an issue addressed in a subsequent paper [24].

5.2.6. Length of hydrocarbon tail

The effect of the length of the long hydrocarbon tail on the ammonium ion can be seen by comparing the $(HE)_2M_1C_1^*$, $(HE)_2M_1T_1$, and $(HE)_2M_1R_1$ structures. Each WAXS curve, shown in Fig. 15, is relatively smooth without any characteristic Bragg reflection. Comparison of TEM photomicrographs for these nanocomposites show highly exfoliated platelets dispersed within the nylon 6 matrix, as seen in Figs. 10(b), 15(a) and (b). Increasing the average alkyl carbon number from 12 to 18 to 22 appears to have no significant effect on the final composite morphology.

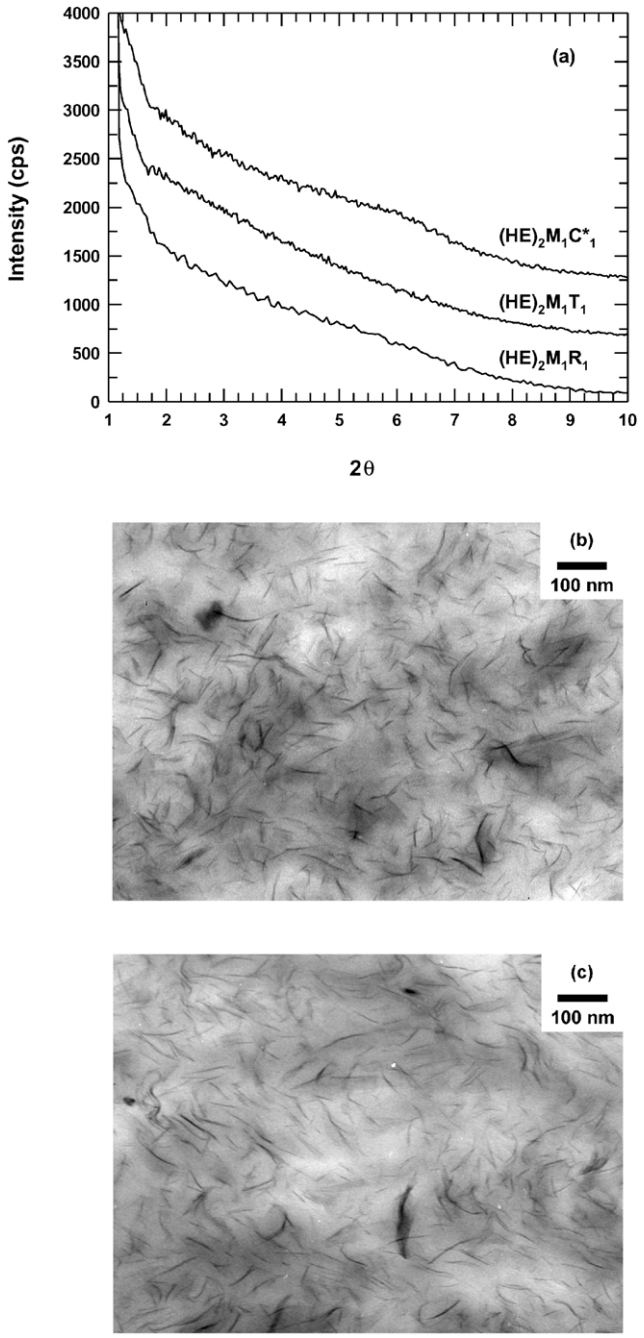

Fig. 15. Morphological analysis of nanocomposites based on HMW nylon 6 and the organoclays whose ammonium ion structure differ only in alkyl tail length. (a) WAXS scans of nanocomposites based on the organoclays $(HE)_2M_1C_1^*$, $(HE)_2M_1T_1$, and $(HE)_2M_1R_1$ and TEM photomicrographs of (b) $(HE)_2M_1C_1^*$, and (c) $(HE)_2M_1R_1$ based composites. The $(HE)_2M_1C_1^*$, and $(HE)_2M_1T_1$, nanocomposites contain 2.8 wt% MMT, while the $(HE)_2M_1R_1$ based composite contains 3.2 wt% MMT. The WAXS scans have been shifted vertically for clarity.

Mechanical properties for these nanocomposites show similar trends, as presented in Fig. 13(d,d′). Modulus curves for the rapeseed ($\sim C_{22}$) and coco ($\sim C_{12}$) are nearly identical, while the tallow systems dominates at the lower MMT concentration. Elongation at break data, shown in Fig. 13(d′), again reveal very similar behavior for the

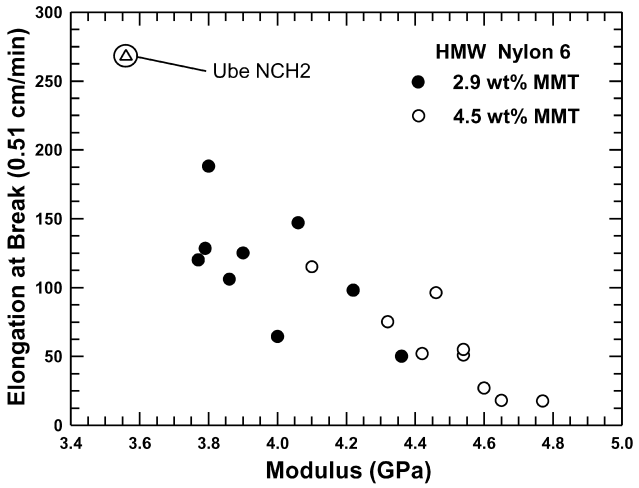

Fig. 16. Ductility-modulus tradeoff curve for nanocomposites based on the various organoclays and HMW nylon 6 for a fix MMT contents of 2.9 and 4.5 wt%. The triangle represents the NCH2 nanocomposite from Ube Industries formed by in situ polymerization. NCH2 pellets, having a silicate concentration of 1.9 wt% MMT, were injection molded and subsequently tested using the same experimental protocol as what used for the melt processed nanocomposites.

$(HE)_2M_1R_1$ and $(HE)_2M_1C_1^*$ composites. Surprisingly, the $(HE)_2M_1T_1$ system holds a slight advantage in ductility despite the higher stiffness value at the low MMT loading level. Comparison of yield strengths between the three types of nanocomposites does reveal a slight decrease in strength with increasing carbon number (Tables 1 and 3); this behavior is somewhat expected based on the influence of pristine organoclay *d*-spacing on yield strength as seen earlier in Fig. 5(b). However, the differences in *d*-spacing for these organoclays are small. Collectively, the above results do not indicate any significant effects of alkyl chain length on nanocomposite morphology or properties for the range of lengths examined. Other studies on polypropylene and epoxy [20,23] demonstrated little, if any, effect of tail length on exfoliation so long as the alkyl contained 12 or more carbon atoms. These investigations were based on the use of pure alkyl chains, while the comparisons made here involve organoclays that are not based on simple alkyls but tails having a distribution of chain lengths containing some unsaturation.

Fig. 16 summarizes the mechanical properties of all melt processed nanocomposites formed from HMW nylon 6 and the various organoclays as well as a single data point corresponding Ube NCH2. Pellets of the latter were injection molded into tensile bars and tested using the same experimental protocol as described earlier. A wide range of properties is obtainable depending upon the type of organoclay used and the loading level. For example, organoclays having one long hydrocarbon tail on the surfactant typically lead to high reinforcement, but lower ductility, while two-tailed surfactants often result in more ductile, less stiff nanocomposites. However, in general, nanocomposite ductility and stiffness follow a linear tradeoff relationship (Fig. 16), regardless of loading level. The deviations from this general trend may be significant in selecting the type of organoclay for a given application.

Table 5
Modulus data for selected nanocomposites formed from LMW nylon 6

LMW–organoclay nanocomposite	Modulus[a] (GPa)
Virgin LMW nylon 6–0.0 wt% MMT	2.82
$M_3(HT)_1$–2.9 wt% MMT	3.86 (3.86)
$M_3(HT)_1$–4.4 wt% MMT	4.18 (4.20)
$M_2H_1(HT)_2$–3.2 wt% MMT	3.62 (3.53)
$M_2H_1(HT)_2$–4.6 wt% MMT	4.01 (3.98)
$M_2(HT)_2$-95–3.2 wt% MMT	3.68 (3.61)
$M_2(HT)_2$-95–4.4 wt% MMT	3.96 (3.99)
$M_2(HT)_2$-125–3.1 wt% MMT	3.50 (3.45)
$M_2(HT)_2$-125–4.5 wt% MMT	3.86 (3.86)

[a] Values in parenthesis represent data interpolated/extrapolated to the target values of 2.9 and 4.5 wt% MMT.

6. Organoclay structure–LMW nanocomposite property relationships

In a recent publication, we showed that higher molecular grades of nylon 6 were more effective at exfoliating $(HE)_2M_1R_1$ than a low molecular weight grade, designated as LMW [18,19] (Section 2.1). This effect was attributed to the higher melt viscosity and consequently higher shear stresses during extrusion compounding associated with the higher molecular weight polyamides. The materials described earlier were made from the highest molecular weight nylon 6 in this series; thus, the effect of the organoclay chemistry was tested in the best possible rheological or processing situation. It is useful to see if the conclusions are altered when the rheology or processing is not optimal. Consequently, some comparisons are made using the lowest molecular weight nylon 6 in the above-mentioned series. Actual and interpolated modulus data for selected nanocomposites based on the LMW nylon 6 are given in Table 5. Fig. 17 shows a plot of modulus versus wt% MMT for three different nanocomposites based on $M_3(HT)_1$, $M_2(HT)_2$-95, and $M_2(HT)_2$-125 organoclays. The graph illustrates that increasing the number of alkyl tails from one to two, viz. $M_3(HT)_1$ to $M_2(HT)_2$-95, and increasing the level of organic loading, $M_2(HT)_2$-95 to $M_2(HT)_2$-125, results in a drop in modulus. Since modulus is a strong indicator of platelet exfoliation, it would be reasonable to rate these surfactants as $M_3(HT)_1 > M_2(HT)_2$-95 $> M_2(HT)_2$-125 in terms of exfoliation efficiency. Both effects are believed to follow the same logic as outlined earlier for the HMW nylon 6.

This section further illustrates the effect of nylon 6 matrix molecular weight on the morphology and properties of nanocomposite formed by melt processing. Fig. 18 compares WAXS scans of nanocomposites based on LMW and HMW nylon 6 formed from two types of organoclays,

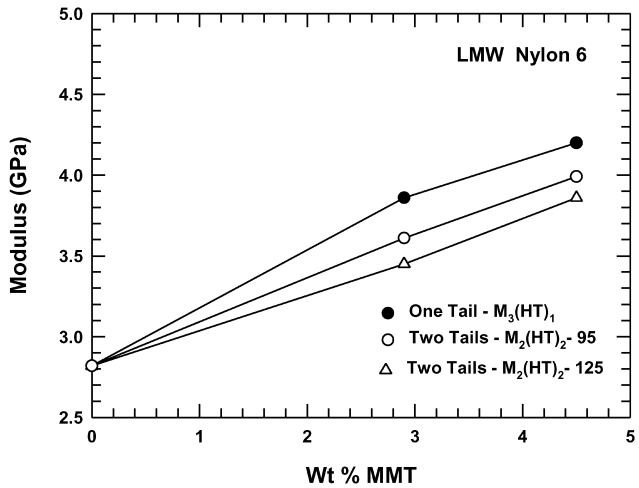

Fig. 17. The effect of number of alkyl tails and organic modifier loading on modulus for nanocomposites based on LMW nylon 6 and the quaternary alkyl ammonium organoclays $M_3(HT)_1$, $M_2(HT)_2$-95, and $M_2(HT)_2$-125.

$M_3(HT)_1$ and $M_1H_1(HT)_2$. The nanocomposites based on HMW nylon 6 (Fig. 18(a) and (b)) have smooth WAXS curves, showing no Bragg reflections, unlike the composites based on LMW nylon 6. Interestingly, the reflection seen in Fig. 18(b) for the LMW-$M_1H_1(HT)_2$ system occurs at a *d*-spacing of 21 Å, slightly below the pristine organoclay *d*-spacing of 24.3 Å. We believe this is an indicative of degradation of the ammonium ion within the galleries of the clays. It is speculated that the silicate platelets quickly exfoliate in the HMW nylon 6 before significant surfactant degradation can occur. The exfoliation time scale in LMW nylon 6, on the other hand, is longer and, thus, competes with the degradation process.

Mechanical property data for nanocomposites formed from HMW and LMW nylon 6 using these two organoclays are presented in Fig. 19. The higher matrix molecular weight leads to a higher modulus at each MMT concentration as shown previously [18,19]; similar trends in morphology and mechanical properties have been observed for other organoclays tested. Therefore, it can be concluded that HMW nylon 6 is consistently more effective at exfoliating organically modified montmorillonite during melt processing than the LMW nylon 6.

7. Conclusions

Structure–property relationships for nanocomposites formed by melt processing from a series of organically modified montmorillonite clays and high and low molecular weight grades of nylon 6 are presented here. The structure of the alkyl ammonium on the clay was systematically varied to determine how specific groups affect polyamide nanocomposite morphology and physical properties. As seen by WAXS, galleries of the organoclays expand in a systematic manner to accommodate the molecular size and the amount of amine surfactant exchanged for the inorganic cation of

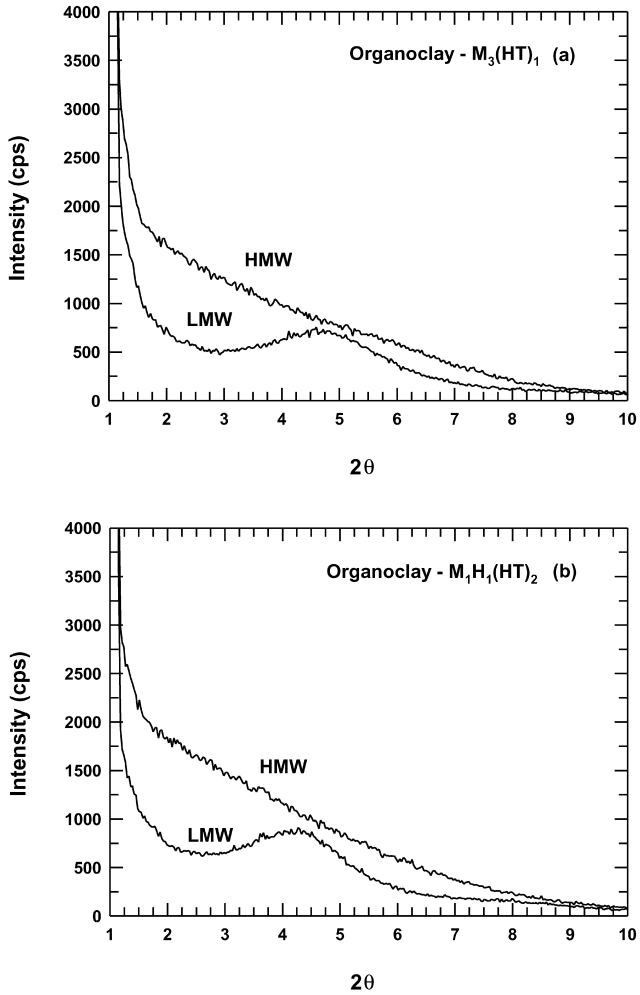

Fig. 18. WAXS patterns for nanocomposites based on LMW and HMW nylon 6 and (a) $M_3(HT)_1$ and (b) $M_2H_1(HT)_1$. The nanocomposites from $M_3(HT)_1$ both contain 2.9 wt% MMT, while the LMW and HMW versions of the $M_2H_1(HT)_1$ nanocomposite contain 2.9 and 2.8 wt% MMT, respectively.

the native montmorillonite. A quantitative analysis shows that the density of the organic material in the galleries is in the range expected for organic liquids and solids. Both the modulus and the yield strength of the nanocomposites seem to decrease as the original organoclay *d*-spacing increases in contrast to some earlier suggestions in the literature. This trend seen in Fig. 5 may not be general, but may reflect issues specific to the surfactants included in this study already discussed in detail.

Three distinct surfactant structural effects have been identified that lead to greater extents of exfoliation, higher stiffness, and increased yield strengths for nanocomposites based on the high molecular weight polyamide. (1) One long alkyl tail on the ammonium ion rather than two, (2) methyl groups on the amine rather than 2-hydroxy-ethyl groups, and (3) an equivalent amount of amine surfactant on the clay as opposed to an excess amount. Similar trends, but lower extents of exfoliation, were seen for a low molecular weight grade (LMW) of nylon 6. It is proposed that these effects

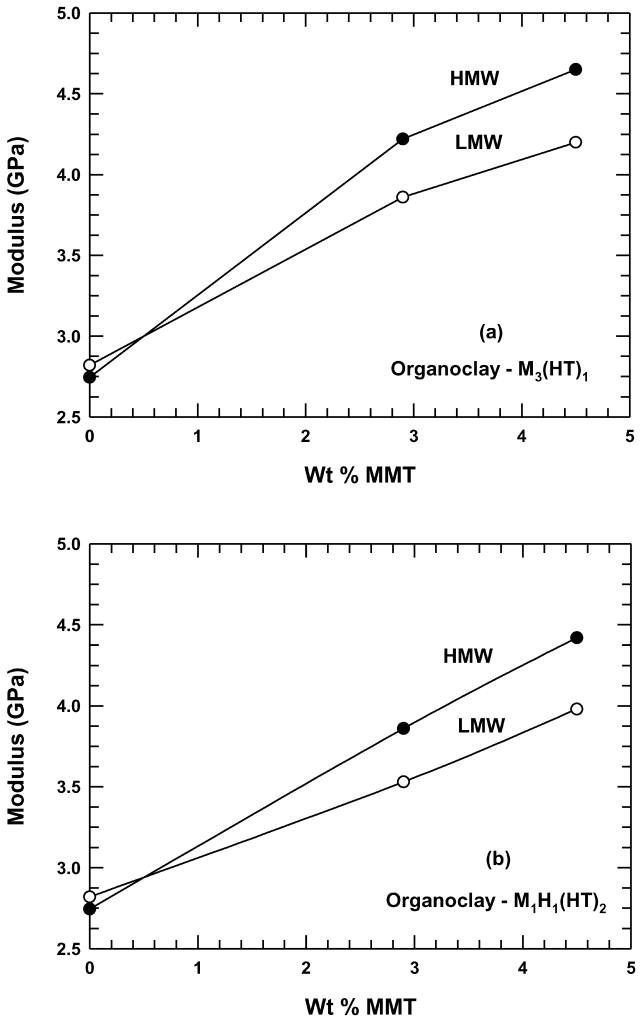

Fig. 19. The effect of nylon 6 matrix molecular weight on modulus of nanocomposites based on (a) $M_3(HT)_1$ and (b) $M_2H_1(HT)_1$.

stem from the amount of exposed silicate surface. Alkyl ammonium ions that cover a larger percentage of the silicate surface, shield desirable polar polyamide–polar clay interactions and ultimately lead to less platelet exfoliation. This proposal, however, does not imply that unmodified clay, i.e. sodium montmorillonite, would be optimum. Organic modification of the clay is required to overcome the cohesive forces between neighboring platelets so that polymer intercalation and platelet exfoliation can occur during melt processing. It should also be emphasized that the effects observed in this work may be specific to nylon 6 matrices; thus, the nature of polymer–organoclay thermodynamic interactions may be different for other polymer matrices and may lead to different structure–property effects.

Lastly, the matrix molecular weight of the polyamide has a significant effect on nanocomposite morphology and mechanical properties. The higher molecular weight polyamide consistently leads to better exfoliation and greater reinforcement than lower molecular weight polyamides; this effect was first seen in a study limited to a single organoclay [18,19]. From these studies, it is clear that with proper selection of the nylon 6, organoclay modifier, and processing procedure can lead to attractive nanocomposites by melt processing [13,17–19].

Acknowledgments

This work was supported by the Texas Advanced Technology Program under grant number 003658-0067 and by the Air Force Office of Scientific Research. The authors would like to especially thank Randy Chapman and Ryan Dennis of Southern Clay Products and Peggy Miller of The University of Texas Health Science Center in San Antonio for their help with WAXS and TEM analyses.

References

[1] Alexandre M, Dubois P. Mater Sci Engng 2000;28:1–63.
[2] Okada A, Fukushima Y, Kawasumi M, Inagaki S, Usuki A, Sugiyami S, Kurauchi T, Kamigaito O. US Patent No. 4,739,007; 1988 (assigned to Toyota Motor Co., Japan).
[3] Usuki A, Kojima Y, Kawasumi M, Okada A, Fukushima Y, Kurauchi T, Kamigaito O. J Mater Res 1993;8(5):1179–84.
[4] Christiani BR, Maxfield M. US Patent No. 5,747,560; 1998 (assigned to AlliedSignal, Inc).
[5] Liu L, Qi Z, Zhu X. J Appl Polym Sci 1999;71(7):1133–8.
[6] Weimer MW, Chen H, Giannelis EP, Sogah DY. J Am Chem Soc 1999;121(7):1615–6.
[7] Yano K, Usuki A, Okada A, Kurauchi T, Kamigaito O. J Polym Sci, Part A: Polym Chem 1993;31(10):2493–8.
[8] Yano K, Usuki A, Okada A. J Polym Sci, Part A: Polym Chem 1997; 35(11):2289–94.
[9] Delozier DM, Orwoll RA, Cahoon JF, Johnston NJ, Smith JG, Connell JW. Polymer 2001;43(3):813–22.
[10] Messersmith PB, Giannelis EP. Chem Mater 1994;6(10):1719–25.
[11] Lan T, Pinnavaia TJ. Chem Mater 1994;6(12):2216–9.
[12] Wang Z, Pinnavaia TJ. Chem Mater 1998;10(7):1820–6.
[13] Cho JW, Paul DR. Polymer 2001;42(3):1083–94.
[14] Rose J. Modern Plast 2001;(October):37.
[15] Haughey J. Modern Plast 2002;(February):34.
[16] Garces JM, Moll DJ, Bicerano J, Fibiger R, McLeod DG. Adv Mater 2000;12(23):1835–9.
[17] Dennis HR, Hunter DL, Chang D, Kim S, White JL, Cho JW, Paul DR. Polymer 2001;42(23):9513–22.
[18] Fornes TD, Yoon PJ, Keskkula H, Paul DR. Polymer 2001;42(25): 9929–40.
[19] Fornes TD, Yoon PJ, Keskkula H, Paul DR. Polymer 2002;43(7): 2121–2.
[20] Reichert P, Nitz H, Klinke S, Brandsch R, Thomann R, Mulhaupt R. Macromol Mater Engng 2000;275:8–17.
[21] Usuki A, Kawasumi M, Kojima Y, Okada A, Kurauchi T, Kamigaito O. J Mater Res 1993;8(5):1174–8.
[22] Okada A, Usuki A. Mater Sci Engng 1995;C3:109–15.
[23] Lan T, Kaviratna PD, Pinnavaia TJ. Chem Mater 1995;7(11): 2144–50.
[24] Fornes TD, Yoon PJ, Paul DR. In preparation.
[25] Van Olphen H. An introduction to clay colloid chemistry, 2nd ed. New York: Wiley/Interscience; 1977.
[26] Vaia RA, Teukolsky, RK, Giannelis, EP. Chem Mater 1994; 6(7):1017–22.

[27] Gelfer MY, Burger C, Hsiao BS, Chu B, Song HH, Avila-Orta C, Liu L, Si M, Rafailovich M. Polym Mater Sci Engng 2001;85:16–17.
[28] Kojima Y, Usuki A, Kawasumi M, Okada A, Fukushima Y, Kurauchi T, Kamigaito O. J Mater Res 1993;8(5):1185–9.
[29] Miller JC, Miller JN. Statistics for analytical chemistry. New York: Wiley; 1984.
[30] Clegg DW, Collyer AA. Mechanical properties of reinforced thermoplastics. New York: Elsevier; 1986. p. 258–65.
[31] Laura DM, Keskkula H, Barlow JW, Paul DR. In press.
[32] Vaia RA, Giannelis EP. Macromolecules 1997;30(25):7990–9.
[33] Vaia RA, Giannelis EP. Macromolecules 1997;30(25):8000–9.
[34] Tanaka G, Goettler LA. Polymer 2001;43(2):541–53.
[35] Masenelli-Varlot K, Reynaud E, Vigier G, Varlet J. J Polym Sci, Part B: Polym Phys 2002;(40):272–83.
[36] Lee S-S, Lee CS, Kim M-H, Kwak SY, Park M, Lim S, Choe CR, Kim J. J Polym Sci, Part B: Polym Phys 2001;(39):2430–5.